A Nano-Scale Multi-Asperity Contact and Friction Model

George G. Adams, Sinan Müftü and Nazif Mohd Azhar

Department of Mechanical, Industrial and Manufacturing Engineering, 334 SN

Northeastern University

Boston, MA 02115, USA

Submitted to *Journal of Tribology, ASME Transactions,* for review

September 2002

Abstract

As surfaces become smoother and loading forces decrease in applications such as MEMS and NEMS devices, the asperity contacts which comprise the real contact area will continue to decrease into the nano scale regime. Thus it becomes important to understand how the material and topographical properties of surfaces contribute to measured friction forces at this nano scale.

In this investigation, the single asperity nano contact model of Hurtado and Kim is incorporated into a multi-asperity model for contact and friction which includes the effect of asperity adhesion forces using the Maugis-Dugdale model. The model spans the range from nano-scale to micro-scale to macro-scale contacts. Three key dimensionless parameters have been identified which represent combinations of surface roughness measures, Burgers vector length, surface energy, and elastic properties. Results are given for the friction coefficient vs. normal force, the normal and friction forces vs. separation, and the pull-off force for various values of these key parameters.

Keywords: friction coefficient; contact; nanocontacts; multi-asperity models.

Nomenclature

A = real contact area
A_M = Maugis model contact radius
$\hat{A}$ = contact radius correction factor
B = y-intercept of region-2 of HK
E = Young's modulus
E^* = composite Young's modulus
F = friction force
F_f = friction force on a single asperity
$\overline{F}$ = dimensionless shear force
G = shear modulus
G^* = effective shear modulus
K = plane stress correction factor
M = slope of curve in region-2 of HK
N = number of asperities
P = normal force
$\overline{P}$ = dimensionless normal force
P_M = Maugis model normal force
$\hat{P}$ = normal force correction factor
R = radius of asperity curvature
a = contact radius
$\overline{a}$ = dimensionless contact radius
b = Burgers vector magnitude
c = adhesion contact radius
d = separation
$\overline{d}$ = dimensionless separation
h = maximum adhesion distance
k = scaling factor
m = ratio of the radii of the adhesion region to the Hertz contact region
u = normal approach
$\overline{u}$ = dimensionless normal approach
w = surface energy of adhesion
z = asperity height
$\overline{z}$ = dimensionless asperity heights
α = surface roughness parameter
β = friction regime parameter
γ = surface energy/compliance coefficient
$\hat{\delta}$ = normal approach correction factor
Δ_M = Maugis model penetration
λ = dimensionless adhesion parameter
μ = static coefficient of friction
ν = Poisson's ratio
σ = standard deviation of asperity peak heights
σ_o = adhesive tensile stress
τ_f = friction stress
τ_{f_1}, τ_{f_2} = shear stress at upper and lower limits of the HK model
ϕ = asperity peak probability distribution

Introduction

Contact and friction affect the operation of many machines and tools we use every day, as well as some of the most basic activities in nature. Examples range from belt drives, brakes, tires, clutches, in automobiles and in other machines; gears, bearings and seals in a variety of mechanical systems; electrical contacts in motors; slider-disk interactions in a disk drive; MEMS motors; a robotic manipulator joint; the motion of a human knee-joint (natural or artificial); and walking/running on the ground. From these examples it is clear that friction can be beneficial (e.g. brakes, tires, walking) or detrimental (e.g. bearings, seals, robotic or human joints). Friction can also be classified as dynamic (e.g. sliding contact in brakes, slider-disk interactions, motion of joints) or predominately static (i.e. little, if any, relative motion, which may include micro-slip as in rolling of train wheels, belt drives, and walking). Friction may also be classified as dry (i.e. without an intervening lubricant as with brakes, tires, and walking) or lubricated (e.g. slider-disk interactions, bearings, and human joints).

The friction force F is the tangential force resisting the relative motion of two surfaces which are pressed against each other with a normal force P. Amontons, in 1699, and Coulomb in 1785, developed our phenomenological understanding of *dry* friction between two contacting bodies. Amontons-Coulomb friction states that the ratio of the friction force (during sliding) to the normal force acting is a constant called the *coefficient of kinetic friction.* Similarly the *coefficient of static friction* is the ratio of the maximum friction force that the surfaces can sustain, without relative motion, to the normal force. Experiments show that static friction is somewhat greater than dynamic friction. We can summarize these friction laws by defining the coefficient of friction μ as

$$\mu = \frac{F}{P} \tag{1}$$

without distinguishing between static and low-speed sliding friction. Although Eq. (1) provides an extraordinarily simple phenomenological friction law, the *nature* of the friction force is not at all well-understood.

Tabor [1] reviewed the state of understanding of friction phenomenon as it existed two decades ago. Friction was originally thought to be due to the resistance of asperities on one surface riding over the asperities of the mating surface. The distinction between static and dynamic friction was attributed to the asperities jumping over the gap between neighboring asperities on the other surface during sliding. The main criticism of this *roughness theory of friction* is that it is a conservative process whereas friction is known to be dissipative. Nonetheless the terminology of "smooth" and "rough" to represent frictionless and frictional contact respectively still persists in, for example, many elementary mechanics textbooks.

The *adhesion theory of friction* relates roughness to friction in a different manner [1]. Because real surfaces always possess some degree of roughness (Fig. 1), the contact between two bodies occurs at or near the peaks of these contacting asperities. Thus the real area of contact will generally be much less than the apparent contact area and the average normal stress in the real contact area can easily exceed the material hardness. If each asperity contact is viewed as a plastic indentation, then the normal contact stress is constant, and the real area of contact is proportional to the normal force. Thus the adhesion theory of friction, which gives a friction force proportional to the real contact area, also gives the required proportionality between the friction force and the normal load for Amontons-Coulomb friction, i.e. Eq. (1). However even in the absence of plastic deformation, the real area of contact is nearly proportional to the normal load if the asperities have a statistical distribution of heights (Geeenwood and Williamson, [2]). Thus Tabor [1] lists the following three basic elements contributing to the friction of unlubricated solids: (1) the real contact area between the sliding surfaces; (2) the type and the

strength of the bond at the contact interface; and (3) the shearing and rupturing characteristics of the material in and around the contact regions. These basic elements can be strongly affected by various factors such as the presence of oxide films, the contact size of individual asperities, and temperature effects.

Consequently, *contact modeling* becomes an essential part of any friction model. It consists of two related steps. First, the equations representing the contact of a single pair of asperities are determined. In general this procedure includes elastic, elastic-plastic, or completely plastic deformation. Depending on the scale of the contact, plasticity effects may be penetration-depth dependent (Hutchinson, [3]). For nanometer scale contacts the effect of adhesion on the contact area is important. Second, the cumulative effects of individual asperities are determined. Conventional multi-asperity contact models may be categorized as predominately uncoupled or predominately coupled. *Uncoupled* contact models represent surface roughness as a set of asperities, often with statistically distributed parameters. The effect of each individual asperity is local and considered separately from the other asperities; the cumulative effect is the summation of the actions of individual asperities. *Coupled* models include the effect of the loading on one asperity on the deformation of neighboring asperities. Such models are far more complex mathematically than the uncoupled models and for that reason have been used less frequently.

The well-known solution for the single contact area between two elastic bodies was developed in the late nineteenth century by Hertz. The assumptions for what has become known as the Hertz contact problem are: (1) the contact area is elliptical; (2) each body is approximated by an elastic half-space loaded over an elliptical contact area; (3) the dimensions of the contact area must be small compared to the dimensions of each body and to the radii of curvature of the surfaces; (4) the strains are sufficiently small for linear elasticity to be valid; and (5) the contact is frictionless, so that only a normal pressure is transmitted. For the case of solids of revolution, the contact area is circular. The interference, contact radius, and maximum contact pressure are given by simple equations [4] which depend upon the Young's moduli, the Poisson's ratios, the radii of curvature, and the applied force.

Various statistical models of multi-asperity contact have been developed in order to determine the normal contact force, many of which are related in some way to the pioneering work of Greenwood and Williamson (GW) [2]. The GW model assumes that in the contact between one rough and one smooth surface: (1) the rough surface is isotropic; (2) asperities are spherical near their summits; (3) all asperity summits have the same radius of curvature while their heights vary randomly; (4) there is no interaction between neighboring asperities; and (5) there is no bulk deformation. The first three assumptions were relaxed by McCool [5] who treated anisotropic rough surfaces with ellipsoidal asperities. However his results were in good agreement with the simpler GW model. Greenwood and Tripp [6] showed that the contact of two rough surfaces can be replaced with the contact of a single rough body with a smooth surface.

For sufficiently small size contacts, the normal adhesion forces between the surfaces affect the contact conditions. Various adhesion models, between an elastic sphere and a flat, have been introduced. The model by Johnson, Kendall and Roberts (JKR) assumes that the attractive intermolecular surface forces cause elastic deformation beyond that predicted by the Hertz theory, and produces a subsequent increase of the contact area [7]. This model also assumes that the attractive forces are confined to the contact area and are zero outside the contact area. The model by Derjaguin, Muller and Toporov (DMT), on the other hand, assumes that the contact area does not change due to the attractive surface forces and remains the same as in the Hertz theory [8]. In this model the attractive forces are assumed to act only outside of the contact area. Due to the assumptions involved, the JKR model is more suitable for soft materials

and the DMT model is more appropriate for harder materials. Another model, introduced by Maugis [9], describes a continuous transition between the JKR and DMT models [10]. In order to represent the surface forces, Maugis used a Dugdale approximation [11] in which the attractive stress is a constant σ_0 for surface separations up to a prescribed value *h*. Intimate contact is maintained over a central region of radius $0 \le r \le a$, an adhesive stress of constant magnitude σ_0 acts outside the contact zone in $a \le r \le c$, and the region $r > c$ is stress-free.

Models to predict the friction force in a multi-asperity contact are relatively few. In the first of a series of papers Chang, Etsion and Bogy (CEB) [12] developed an elastic-plastic multi-asperity contact model for normal loading based on volume conservation of a plastically deformed asperity control volume. In [13], the effect of adhesion was included in the multi-asperity contact model of [12] by using the DMT model for contacting asperities and the Lennard-Jones potential between non-contacting asperities. The DMT model was used because it was thought to be appropriate for the contact of hard metal surfaces. The effects of the surface energy of adhesion and of the surface roughness, on the adhesion force and on the pull-off force were examined. Finally a model for calculating the coefficient of friction was given in [14]. It assumed that once plastic yielding is initiated in a pair of contacting asperities, no further tangential force can be sustained. In order to calculate this limiting shear force, the stress field for an asperity subject to normal and lateral tractions developed by Hamilton [15] was used. For a given normal load, the maximum tangential force that can be sustained before the initiation of plastic yielding (based upon the von Mises yield criterion) was calculated. Thus any asperity which was plastically deformed under normal loading cannot resist a lateral load. Chang, Etsion and Bogy then calculated the total shear force that a multi-asperity interface can sustain by integrating the shear force relation statistically as in the GW model. They showed that the static coefficient of friction decreases with increasing plasticity index and that it increases with increasing surface energy. Also as the external normal force increases, the static friction coefficient decreases. This latter result is contrary to ordinary Amonton-Coulomb friction, but consistent with the results of various experimental investigations cited in [14].

Fuller and Tabor [16] investigated the effect of roughness on the adhesion between elastic bodies. Experiments were conducted between rubber spheres and a hard flat surface with controlled roughness. A theoretical model which used the JKR model of adhesion along with a Gaussian distribution of asperity heights was developed. Their work showed that relatively small surface roughness is sufficient to reduce the adhesion between the surfaces to a very small value. A key parameter was identified which depends on surface energy, composite elastic modulus, standard deviation of asperity heights, and asperity curvature.

Stanley, Etsion and Bogy (SEB) [17] developed a model for the adhesion of two rough surfaces, affected by sub-boundary layer lubrication, in elastic-plastic multi-asperity contact. Sub-boundary lubrication occurs when an extremely thin layer of lubricant is applied to a solid surface and forms a strong bond with the surface, without tending to form menisci. The analysis in [17] showed that even though the introduction of the lubricant reduces the surface free energy, there can be an increase in the overall adhesive force relative to the dry case without the formation of liquid meniscus bridges. A roughness-dependent critical lubricant thickness exists, above which the adhesion force increases rapidly. Polycarpou and Etsion [18] used the SEB model to predict the static friction coefficient in the presence of sub-boundary layer lubrication. The tangential load was found using the same procedure as in the CEB model [14] for solid-solid contact. They found that the coefficient of friction increases with decreasing normal load and that a roughness-dependent critical lubricant thickness exists, above which the adhesion force increases rapidly within the sub-boundary regime.

One of the interesting and important results of the GW model is that the real area of contact is roughly proportional to the normal load. Thus if the friction stress is constant, the friction force is proportional to the real area of contact, and hence the friction force will be roughly proportional to the normal load. This leads to a coefficient of friction which is nearly independent of normal load. However recent experimental evidence shows that there is a significant change in the friction stress τ_f acting on a single asperity contact, as the contact area changes from the micro to nano scale. Experiments, in which the friction force is measured using an atomic force microscope (AFM) [19], show that the friction stress can be more than an order of magnitude higher as compared to experiments in which the friction is measured with the surface force apparatus (SFA) [20]. A typical contact radius for an AFM tip is estimated to be on the order of 3-14 nm, whereas for SFA it is on the order of 40-250 μm.

The scale dependence of the friction stress has recently been investigated by Hurtado and Kim (HK), [21,22]. They presented a micromechanical dislocation model of frictional slip between two asperities for a wide range of contact radii. According to the HK model, if the contact radius *a* is smaller than a critical value, the asperities slide past each other in a concurrent slip process, where the adhesive forces are responsible for the shear stress; hence the shear stress remains at a high constant value. On the other hand, if the contact radius is greater than the critical value, the shear stress decreases for increasing values of contact radius until it reaches a second constant, but lower value. This behavior is approximated in Fig. 2. In the transition region between the two critical contact radius values, single dislocation assisted slip takes place, where a dislocation loop starts in periphery of the contact region and grows toward the center; the shear stress is dominated by the resistance of the dislocation to motion. Multi-dislocation-cooperated slip is responsible for the friction stress in the second constant shear stress region [21]. It is emphasized that in the HK model the dislocation motion is confined to the interface; hence bulk plastic deformation need not occur.

The HK model provides an expression for the behavior of the friction stress over a wide range of contact areas, including nano scale contacts. In this paper, as in the Adams, Müftü, and Mohd Azhar (AMM) model [23], the frictional slip model of Hurtado and Kim, and the adhesion contact model of Maugis, are combined with the Greenwood and Williamson statistical multi-asperity contact model, in order to derive the relationship between the friction force *F* and the normal load *P* between two rough surfaces during a slip process. The attractive forces between asperities that are not in contact are neglected. The coefficient of friction μ is then calculated as the ratio of the shear force to the applied normal load. Three dimensionless parameters that represent the surface roughness, the friction regime of the contacts, and the surface energy/compliance, are seen to influence the value of the friction coefficient. The effect of varying these three parameters on the coefficient of friction and on the pull-off force is discussed.

Development of the Model

Hurtado-Kim Model

Hurtado and Kim (HK) [21,22] presented a micromechanical dislocation model of frictional slip between two asperities which states that, for contact radii smaller than a critical value, the friction stress is constant. Above that critical value, the friction stress decreases as the contact radius increases until a second transition occurs where the friction stress again becomes independent of the contact size. The relationship between the non-dimensional friction stress $\bar{\tau}_f = \tau_f / G^*$ and the non-dimensional contact radius $\bar{a} = a/b$, according to Hurtado and Kim is given in Fig. 2. The contact radius *a* is normalized by the Burgers vector *b* and the friction stress

τ_f is normalized by the effective shear modulus $G^*=2G_1G_2/(G_1+G_2)$ where G_1 and G_2 are the shear moduli of the contacting bodies. In this figure, region-1 represents typical experimental values obtained using the atomic force microscope (AFM) while region-3 represents the typical experimental values obtained with the surface force apparatus (SFA). These two regions are connected by the transition region-2.

From Fig. 2, the dimensionless shear stress is a function of the dimensionless contact radius and can be approximated by

$$\log\left(\bar{\tau}_f\right)=\begin{cases}\log\bar{\tau}_{f_1}, & \bar{a}<\bar{a}_1\\ M\log\bar{a}+B, & \bar{a}_1<\bar{a}<\bar{a}_2\\ \log\bar{\tau}_{f_2}, & \bar{a}>\bar{a}_2\end{cases} \tag{2}$$

where the left and right limits of region-2 are $\left(\bar{a}_1,\bar{\tau}_{f_1}\right)$ and $\left(\bar{a}_2,\bar{\tau}_{f_2}\right)$ respectively. The constants of Eq. (2) are given by

$$\begin{aligned}M&=-\left(\log\left(\bar{\tau}_{f_1}/\bar{\tau}_{f_2}\right)\right)\Big/\left(\log\left(\bar{a}_2/\bar{a}_1\right)\right)\\ B&=\left(\log\left(\bar{\tau}_{f_1}\right)\log\left(\bar{a}_2\right)-\log\left(\bar{\tau}_{f_2}\right)\log\left(\bar{a}_1\right)\right)\Big/\left(\log\left(\bar{a}_2/\bar{a}_1\right)\right)\end{aligned} \tag{3}$$

The friction force F_f acting on a single asperity can be determined from Eq. (2) by using the relationship $F_f=\pi a^2\tau_f$ as follows

$$\frac{F_f}{G*b^2}=\begin{cases}\bar{\tau}_{f_1}\bar{a}^2, & \bar{a}<\bar{a}_1\\ 10^B\bar{a}^{M+2}, & \bar{a}_1<\bar{a}<\bar{a}_2\\ \bar{\tau}_{f_2}\bar{a}^2, & \bar{a}>\bar{a}_2\end{cases} \tag{4}$$

A Multi-Asperity Friction Model Based on the HK Model

The maximum shear force in the static contact of two asperities can be predicted by the HK model given in Eq. (4). The Greenwood and Williamson model describes the multi-asperity contact of two real rough surfaces [2]. The conditions for which the GW model are valid, given in the Introduction, are assumed to hold here. Then, when two real surfaces are separated by a distance *d* the number of contacting asperities *n* can be found from

$$n=N\int_{\bar{d}}^{\infty}\phi\left(\bar{z}\right)d\bar{z} \tag{5}$$

where *N* is the total number of asperities, σ is the standard deviation of asperity peak heights, $\bar{z}=z/\sigma$ is the dimensionless height coordinate measured from the mean of asperity heights, $\phi\left(\bar{z}\right)$ is the probability density of asperity peaks, and $\bar{d}=d/\sigma$ is the non-dimensional separation between the two surfaces. The general relation between the normal load *P* and the deformation *u* of two spherical asperities in contact is given by the Hertz contact theory as $P=\left(4/3\right)E^*R^{1/2}u^{3/2}$, where *R* is the composite radius of curvature of the asperity tips, and E^* is the composite Young's modulus of the two materials [4]. In this work, one of the surfaces is assumed to be rigid and flat. Thus the composite Young's modulus is given by $E^*=E/(1-\nu^2)$ and $G^*=2G$ where ν, *E*, *G* are the Poisson's ratio, Young's modulus, and shear modulus of the elastic body respectively. The total deformation *u* of the asperities is equal to the penetration, i.e. $u=z-d$, as shown in Fig. 1.

Thus the GW model gives the non-dimensional normal force per asperity $\overline{P}$ between two nominally flat, otherwise rough surfaces, separated by a distance $\overline{d}$ as

$$\overline{P} = \frac{P}{NGb^2} = \frac{4}{3}\frac{2}{1-\nu}\alpha\beta^2\int_{\overline{d}}^{\infty}\left(\overline{z}-\overline{d}\right)^{3/2}\phi\left(\overline{z}\right)d\overline{z} \tag{6}$$

In Eq. (6), the two non-dimensional surface parameters α and β have been defined as

$$\alpha = \left(\frac{\sigma}{R}\right)^{1/2}, \qquad \beta = \frac{\left(R\sigma\right)^{1/2}}{b}, \tag{7}$$

and the relation $G=E/2(1+\nu)$ has been used. For Hertz contact, the dimensionless relations for a single asperity contact are

$$\overline{a} = \frac{(Ru)^{1/2}}{b} = \beta\left(\overline{z}-\overline{d}\right)^{1/2} \quad \text{or} \quad \overline{z} = \overline{d} + \frac{\overline{a}^2}{\beta^2}. \tag{8}$$

In order to provide a physical interpretation of the surface parameters α and β, it is noted that in a simple vertical scaling of the surface by a factor k, the standard deviation of asperity heights σ is scaled by k but the asperity radius of curvature R is scaled by $1/k$. Thus, α is scaled by k, but β remains constant. Hence α is a representation of the surface roughness, and will be referred to as a *surface roughness parameter*. The parameter β describes the ratio of the contact radius (due to a penetration equal to σ) to the Burgers vector length. Thus small β are expected to be indicative of nano scale asperity contacts and progressively larger values of β correspond to transition and larger values of the contact radius (Fig. 2). Therefore β will be referred to as the *friction regime parameter*.

The total shear force F acting on the nominal contact area can be calculated integrating the shear forces acting on each asperity against the probability density function

$$F = N\int_{\overline{d}}^{\infty} F_f\phi\left(\overline{z}\right)d\overline{z}\,. \tag{9}$$

In non-dimensional form, the force per asperity $(\overline{F})$ becomes, using Eqs. (4) and (9),

$$\overline{F} = \frac{F}{NGb^2} = 2\pi\overline{\tau}_{f_1}\int_{\overline{d}}^{\overline{z}_1}\overline{a}^2\phi\left(\overline{z}\right)d\overline{z} + 2\pi 10^B\int_{\overline{z}_1}^{\overline{z}_2}\overline{a}^{M+2}\phi\left(\overline{z}\right)d\overline{z} + 2\pi\overline{\tau}_{f_2}\int_{\overline{z}_2}^{\infty}\overline{a}^2\phi\left(\overline{z}\right)d\overline{z} \tag{10}$$

The constants $\overline{\tau}_{f_1}$ and $\overline{\tau}_{f_2}$ are described in Eq. (2); the integration limits $\overline{z}_1$ and $\overline{z}_2$ are determined from Eq. (2) and Eq. (8); and the contact radius $\overline{a}$ is a function of $\overline{z}$ according to Eq. (8). Thus, the coefficient of friction μ for two real surfaces separated by a distance $\overline{d}$, can be obtained from Eqs. (1), (6) and (10). Note that the relationship between the scaled coefficient of friction $(\alpha\mu)$ and the scaled normal force $(\overline{P}/\alpha)$ depends only on the friction regime parameter (β).

Adhesion Effects in the Multi-Asperity Contact and Friction Model

In the contact of two bodies, the adhesive stresses between the two surfaces affects the contact conditions. For micro-scale or larger contacts these effects are negligible, whereas at the nano-scale adhesion becomes important. Adhesive effects in the elastic contact of two spheres, are included in the JKR model, which is suitable for soft surfaces, and in the DMT model, which is appropriate for hard surfaces. In the present investigation, we use the Maugis model of elastic adhesive contact, which uses a Dugdale approximation of the adhesive stresses and is applicable over the entire range of material properties. In the Dugdale approximation, a uniform tensile stress σ_0 exists between the contacting asperities just outside the contact zone, $a \le r \le c$, where

c is the extent of the adhesion zone in the radial direction. The separation between the two surfaces at $r = c$ is equal to the prescribed maximum adhesion distance h. In [9] the following non-dimensional relations among asperity contact radius (A_M), asperity contact force (P_M), and asperity deformation (Δ_M) were obtained

$$\frac{\lambda A_M^{\,2}}{2}\left[\sqrt{m^2-1}+\left(m^2-2\right)\tan^{-1}\sqrt{m^2-1}\right]+\frac{4\lambda^2 A_M}{3}\left[\sqrt{m^2-1}\tan^{-1}\sqrt{m^2-1}-m+1\right]=1 \tag{11}$$

$$P_M = A_M^{\,3}-\lambda A_M^{\,2}\left[\sqrt{m^2-1}+m^2\tan^{-1}\sqrt{m^2-1}\right] \tag{12}$$

$$\Delta_M = A_M^{\,2}-\frac{4}{3}A_M\lambda\sqrt{m^2-1} \tag{13}$$

where λ is the non-dimensional adhesion parameter, and m is the non-dimensional adhesion radius. The various non-dimensional quantities used in the Maugis model are defined as

$$\begin{gathered} A_M = a\left(\frac{K}{\pi w R^2}\right)^{1/3}, \quad \lambda = 2\sigma_0\left(\frac{R}{\pi w K^2}\right)^{1/3}, \\ m=\frac{c}{a}, \quad P_M=\frac{P}{\pi w R}, \quad \Delta_M = u\left(\frac{K^2}{\pi^2 w^2 R}\right)^{1/3} \end{gathered} \tag{14}$$

where w is the surface energy of adhesion ($w = \sigma_0 h$) and $K = (4/3)\,E^*$.

The simultaneous solution of Eqs. (11)–(13) gives the relations between m, P_M, A_M and Δ_M for a given value of λ. In practice it is convenient to vary m and solve the resulting quadratic equation for the only positive root A_M in (11). Then (12) and (13) can be solved explicitly for P_M and Δ_M respectively. We also express the non-dimensional adhesion parameter λ in terms of the surface roughness parameter α, the friction regime parameter β, the maximum adhesion distance h, Burgers vector b, and the surface energy coefficient γ as

$$\lambda = \left(\frac{b}{h}\right)\left(\frac{9\beta\gamma^2}{2\pi\alpha}\right)^{1/3}, \tag{15}$$

where the surface energy/compliance coefficient (γ) is defined as

$$\gamma = \frac{w}{E^* b}. \tag{16}$$

Note that a high value of γ represents strong adhesion compared to the product of the composite Young's modulus and the Burgers vector.

The non-dimensional variables (A_M, P_M and Δ_M) used in the Maugis model can be expressed in terms of the non-dimensional parameters defined in this work ($\bar{a}, \bar{P}, \bar{u} = u/\sigma$) respectively, according to

$$\bar{u} = \Delta_M \hat{\delta}, \quad \bar{P} = P_M / \hat{P}, \quad \bar{a} = A_M / \hat{A} \tag{17}$$

where

$$\hat{\delta} = \left(\frac{3\pi\gamma}{4\alpha^2\beta}\right)^{2/3}, \quad \hat{P} = \frac{(1-\nu)\alpha^2}{2\pi\beta\gamma}, \quad \hat{A} = \left[\frac{4}{3\pi\gamma}\left(\frac{\alpha}{\beta}\right)^2\right]^{1/3}$$

An expression for the non-dimensional normal force $\bar{P}$ acting on the nominal contact area can be obtained by integrating the normal force on individual asperities from the Maugis model (P_M), as follows

$$\bar{P} = \frac{1}{\hat{P}} \int_{\bar{d}}^{\infty} P_M \phi(\bar{z}) d\bar{z} \,. \tag{18}$$

Adhesion affects the relationship between the normal force and the contact radius, but it does not affect the relation between the friction force and contact radius. The contact radius $\bar{a}$ is used in Eq. (10) to obtain the shear force $\bar{F}$. Then the coefficient of friction for this multi-asperity contact with adhesive effects can be obtained from Eq. (1).

Results and Discussion

Although a variety of surface height distributions may be considered, a Gaussian distribution of asperity peaks, which gives the following probability density function

$$\phi(\bar{z}) = \frac{1}{(2\pi)^{1/2}} \exp\left(-\bar{z}^2/2\right). \tag{19}$$

is chosen. The integrals in Eqs. (6), (10) and (18) were evaluated numerically using MATLAB. For specified λ and a range of values of m, the values of A_M, P_M, and Δ_M were obtained from Eqs. (11)–(13) respectively. In the following, the effects of changing the dimensionless parameters α, β, and γ, on the normal force, the shear force, the friction coefficient, and the pull-off force, are presented. For all of these results, the values of the shear stress and contact radii at the ends of the transition region are $\bar{\tau}_{f_1} = 1/43$, $\bar{\tau}_{f_2} = \bar{\tau}_{f_1}/30$, $\bar{a}_1 = 28$, $\bar{a}_2 = 8\times10^4$ [21].

Figure 3 shows the variation of the coefficient of friction with the normal force when the effect of adhesion between contacting asperities is neglected ($\gamma = 0$). This case corresponds to highly contaminated surfaces and also serves as a baseline for the adhesive contact presented later. In this figure the friction regime parameter β varies in the range $10^2 \le \beta \le 10^6$, whereas the surface roughness parameter α appears only as a scaling factor in the normal force $(\bar{P}/\alpha)$ and in the friction coefficient $(\mu\alpha)$. The scaled coefficient of friction ($\alpha\mu$) is the ratio of the shear force $\bar{F}$ to scaled normal force $(\bar{P}/\alpha)$ and is a convenient quantity to plot because α appears only as a scaling factor. The friction coefficient is observed to be higher for small values of the friction regime parameter β, indicating the importance of the nano friction region of Fig. 2. This difference is especially significant when the normal force is low. Also note that for high β, the friction coefficient becomes less dependent on the normal force. The results given in this figure are attributed to the effects of contact scale; when a greater fraction of the asperities are in contact with smaller contact radii, the result is a higher friction shear stress according to the HK model. At high normal load, the asperity friction force due to the larger contact radii dominate the total friction force even though the friction stress is lower. The effect of increasing α, at fixed normal load, is to increase $\alpha\mu$ somewhat due to the change in the P/α coordinate. However the net effect is that μ varies approximately as the inverse of α.

The effect of adhesion on the friction coefficient is studied next. The coefficient of friction is found from the solution of Eqs. (10)–(12), (17) and (18). The effects of the parameters α, β and γ on the coefficient of friction are investigated in Figs. 4-6. Unless otherwise specified, the values of the parameters are $\alpha = 10^{-2}$, $\beta = 10^3$, $\gamma = 10^{-3}$, and the maximum adhesion distance (h) is taken equal to the Burgers vector length (b).

Figure 4 shows the variation of the friction coefficient with the normal load, for various values of the surface roughness parameter α. Note that the results for different α values are compared to the case where there are no adhesion effects. It is only for α less than about 0.06 that these results differ from the case without adhesion. Small α correspond to lower roughness

as would be expected in micro- and nano-scale applications. As α decreases below 0.01 the effect of adhesion increases significantly. For high loads the effect of the surface roughness represented by α is much less; in fact near $\bar{P}$ = 10^6 the curves approach the same scaled coefficient of friction value.

The effect of the friction regime roughness parameter β on the variation of the friction coefficient with normal force is shown in Fig. 5. The cases in which the adhesion effects are included are plotted with solid lines whereas the cases without adhesion are plotted with broken lines. This figure shows that our model predicts higher coefficients of friction values for lower β values. The effect of adhesion, which is to increase the friction coefficient and the difference between the results with and without adhesion, is greatest for low β and low normal force. Low β indicates that the contacts are more likely to be in the nano region (Fig. 2) in which the friction stress is greatest and the effect of adhesion on the contact radius is expected to be most important. For high β the friction coefficient is nearly independent of adhesion and less sensitive to normal load. A large normal force results in μ being nearly independent of both adhesion and of β. The value of μ decreases with increasing $\bar{P}$. Although it may not at first be obvious from Figs. 3-5, due to the scalings involved, the friction coefficient is more sensitive to α than to β.

Finally, the effect of the adhesion parameter γ on μ vs. $\bar{P}$ is plotted in Fig. 6. A baseline plot without adhesion is also given for comparison. As expected the results show that for high γ, the model predicts higher coefficient of friction values, especially at low loads. It is noted that in each of Figs. 4-6 the friction coefficient decreases with the applied load. Even for a zero value of the applied normal force, the effect of adhesion can be to create a finite contact area and hence a finite friction force which leads to an infinite friction coefficient.

The dimensionless normal force vs. separation is shown in Fig. 7 for various values of α and β, with γ = 10^{-3}. Note that an order of magnitude increase in β produces roughly a two orders of magnitude increase in the normal force. Without adhesion P varies as $\alpha\beta^2$, but with adhesion that relation is more complex. It may appear surprising that the friction regime parameter would have such a strong influence on the normal force. However from Eq. (7)

$$\sigma / b = \alpha\beta \quad \text{and} \quad R / b = \beta / \alpha \tag{20}$$

and so $\alpha\beta^2 = \sigma^{3/2} R^{1/2} / b^2$ which, without adhesion, more explicitly shows the dependence of the normal force with the surface topography (σ,R). The effect of increasing α is to increase the normal force in a nearly linear manner. Note the apparent discontinuity in the curve for α = 0.005, β = 1000. In this case and for a separation (d/σ) of approximately 2.6, the normal force approaches zero. For larger separations, the negative of the normal force has been plotted – the peak value of which indicates the pull-off force. Note that for the five cases plotted only α = 0.005, β = 1000 gives a tensile force on separation.

The dimensionless friction force vs. separation is shown in Fig. 8 for various values of α and β, with γ = 10^{-3}. The trend of a nearly two orders of magnitude increase in the friction force with an order of magnitude increase in the friction regime parameter β appears at first to be counter-intuitive. Note, however, that while an increase in β does cause a decrease in the friction coefficient (Fig. 5) it also causes an increase in both the normal and friction force due to the effect of surface topography, i.e. Eq. (20). The effect of α on the friction force is not as strong, especially at small separations for which the effect of adhesion is less.

The dimensionless average contact pressure (P/E^*A) vs. normal force is shown in Fig. 9 for various values of α and β, with γ = 10^{-3}. The real contact area (A) was computed from

$$A = N\pi b^2 \int_{\bar{d}}^{\infty} \bar{a}^2 \phi(\bar{z}) d\bar{z} = N\pi b^2 \beta^2 \int_{\bar{d}}^{\infty} (\bar{z} - \bar{d}) \phi(\bar{z}) d\bar{z} \tag{21}$$

The solid and dashed lines are with and without adhesion respectively. There is a relatively small change in the average contact pressure as the normal force varies over several orders of magnitude. The effect of adhesion is to reduce the average contact pressure by increasing the real contact area for a given applied load. Also the results are more sensitive to α than to β, with low α (smooth surfaces) giving lower contact pressures due to a greater real contact area.

Finally Table 1 shows the dimensionless pull-off force for various values of the parameters α, β, and γ. As described in connection with Fig. 7, the pull-off force ($|P|/NGb^2$) is the largest magnitude of tensile force needed to separate the surfaces. For most of the material combinations presented, the normal force remains compressive and a pull-off force does not exist. Note that low α and high γ increase the pull-off force dramatically.

Conclusions

The friction force measured between two bodies is the combined result of friction forces which are present in a very large number of nano- and micro-scale asperity contacts. It is known from recent experiments with the AFM and SFA, that single asperity contacts yield friction stresses which have a constant value in the micro range (SFA) but give a constant and much higher value in the nano range (AFM). This difference in friction stress is greater than an order of magnitude. Recent single asperity modeling efforts by Hurtado and Kim [21,22] have demonstrated a mechanism which can explain this phenomenon.

In this paper, the single asperity nano contact model of Hurtado and Kim has been incorporated into a multi-asperity model for contact and friction which includes the effect of asperity adhesion forces using a Maugis model. Three key dimensionless parameters α, β and γ have been defined which represent surface roughness, friction regime, and surface energy/compliance. Results are shown for the friction coefficient vs. the normal load, for the normal and friction forces vs. separation, and for the average contact pressure vs. normal load, for various values of these three key dimensionless parameters. The importance of nano effects in multi-asperity contacts are shown to be most significant for small α and/or β, high γ, and low normal load. Future work should include the effects of scale-dependent plasticity, thin films, various distributions of asperity heights and shapes, asperity coupling, and experiments to validate the model.

References

[1] Tabor, D., 1981, "Friction–The Present State of Our Understanding," *ASME Journal of Lubrication Technology,* **103**, pp. 169-179.

[2] Greenwood, J.A and Williamson, J.B.P., 1966, "Contact of Nominally Flat Surfaces," *Proceedings of the Royal Society of London,* **A295**, pp. 300-319.

[3] Hutchinson, J.W., 2000, "Plasticity at the Micron Scale," International Journal of Solids and Structures, **37**, pp. 225-238.

[4] Johnson, K.L., 1985, *Contact Mechanics*, Cambridge University Press, Cambridge, UK.

[5] McCool, J.I., 1986, "Comparison of Models for the Contact of Rough Surfaces," *Wear*, **107**, pp. 37-60.

[6] Greenwood, J.A., and Tripp, J.H., 1971, "The Contact of Two Nominally Flat Rough Surfaces," *Proceedings of the Institution of Mechanical Engineers*, **185**, pp. 625-633.

[7] Johnson, K. L., Kendall, K., and Roberts, A. D., 1971, "Surface Energy and the Contact of Elastic Solids," *Proceedings of the Royal Society of London,* **A324**, pp. 301-313.

[8] Derjaguin, B. V., Muller, V. M., and Toporov, Y. P., 1975, "Effect of Contact Deformations on the Adhesion of Particles," *Journal of Colloid and Interface Science*, **53**, pp. 314-326.

[9] Maugis, D., 1992, "Adhesion of Spheres: The JKR-DMT Transition Using a Dugdale Model," *Journal of Colloid and Interface Science*, **150**, pp. 243-269.

[10] Johnson, K.L. and Greenwood, J.A., 1997, "An Adhesion Map for the Contact of Elastic Spheres," *Journal of Colloid and Interface Science,* **192**, pp. 326-333.

[11] Dugdale, D. S., 1960, "Yielding in Steel Sheets Containing Slits," *Journal of the Mechanics and Physics of Solids*, **8**, pp. 100-104.

[12] Chang, R. W., Etsion, I., Bogy, D. B., 1987, "An Elastic-Plastic Model for the Contact of Rough Surfaces," *ASME Journal of Tribology*, **109**, pp. 257-263.

[13] Chang, R. W., Etsion, I., Bogy, D. B., 1988, "Adhesion Model for Metallic Rough Surfaces," *ASME Journal of Tribology,* **110**, pp. 50-56.

[14] Chang, R. W., Etsion, I., Bogy, D. B., 1988, "Static Friction Coefficient Model for Metalic Rough Surfaces" *ASME Journal of Tribology*, **110**, pp. 57-63.

[15] Hamilton, G.M., 1983, "Explicit Equations for the Stresses Beneath a Sliding Spherical Contact," *Proceedings of the Institution of Mechanical Engineers,* **197C**, pp. 53-59.

[16] Fuller, K.N.G and Tabor, D., 1975, "The Effect of surface roughness on the adhesion of elastic solids," *Proceedings of the Royal Society of London,* **A345**, pp. 327-342.

[17] Stanley, H.M., Etsion, I. and Bogy, D.B., 1990, "Adhesion of Contacting Rough Surfaces in the Presence of Sub-Boundary Lubrication," *ASME Journal of Tribology*, **112**, pp. 98-104.

[18] Polycarpou, A. A., and Etsion, I.,1998, "Static Friction of Contacting Real Surfaces in the Presence of Sub-Boundary Lubrication," *ASME Journal of Tribology*, **120**, pp. 296-303.

[19] Carpick, R.W., Agrait, N. Ogletree, D.F. and Salmeron, M., 1996, "Measurement of Interfacial Shear (friction) with an ultrahigh vacuum atomic force microscope," *Journal of Vacuum Science and Technology*, **B14**, pp. 1289-1295.

[20] Homola, A.M, Israelachvili, J.N., McGuiggan, P.M. and Gee, M.L., 1990, “Fundamental experimental studies in tribology: the transition from 'interfacial' friction of undamaged molecularly smooth surfaces to 'normal' friction with wear,” *Wear*, **136**, pp. 65-83.

[21] Hurtado, J.A. and Kim, K.-S., 1999, “Scale Effects in Friction of Single Asperity Contacts: Part I; From Concurrent Slip to Single-Dislocation-Assisted Slip,” *Proceedings of the Royal Society of London*, **A455**, pp. 3363-3384.

[22] Hurtado, J.A. and Kim, K.-S.,1999, “Scale Effects in Friction in Single Asperity Contacts: Part II; Multiple-Dislocation-Cooperated Slip,” *Proceedings of the Royal Society of London*, **A455**, pp. 3385-3400.

[23] Adams, G.G., Müftü, S., and Mohd Azhar, N., 2002, “A Nano-Scale Multi-Asperity Model for Contact and Friction,” *2002 ASME/STLE Tribology Conference*, Cancun, Mexico, Oct. 28-30, 2002. Proceedings on CD-ROM. Paper No. ASME2002-TRIB-258.

List of Figures

Figure 1. The topography of a rough surface and a smooth flat surface.

Figure 2. Relationship between the dimensionless friction stress and the dimensionless contact radius according to the HK model.

Figure 3. Scaled coefficient of friction ($\alpha\mu$) vs. scaled normal force ($P/\alpha NGb^2$) for various values of β, without adhesion ($\gamma = 0$).

Figure 4. Scaled coefficient of friction ($\alpha\mu$) vs. scaled normal force ($P/\alpha NGb^2$) for various values of α, with $\gamma = 10^{-3}$.

Figure 5. Coefficient of friction (μ) vs. the dimensionless normal force (P/NGb^2) for various values of the friction regime parameter β, with $\alpha = 0.01$, with adhesion ($\gamma = 10^{-3}$, solid lines) and without adhesion ($\gamma = 0$, dashed lines).

Figure 6. Coefficient of friction (μ) vs. the dimensionless normal force (P/NGb^2) for various values of the surface energy/compliance parameter (γ), with $\alpha = 0.01$ and $\beta = 1000$.

Figure 7. Dimensionless normal force (P/NGb^2) vs. dimensionless separation (σ/d), for various values of α and β, and with $\gamma = 10^{-3}$. Dashed lines indicate that the normal force is tensile.

Figure 8. Dimensionless friction force (F/NGb^2) vs. dimensionless separation (σ/d), for various values of α and β, and with $\gamma = 10^{-3}$.

Figure 9. Dimensionless average contact pressure (P/E^*A) vs. dimensionless normal force (P/NGb^2), for various values of α and β, with $\gamma = 10^{-3}$ (solid lines), and $\gamma = 0$ (dashed lines).

List of Tables

Table 1. Dimensionless pull-off force ($|P|/NGb^2$) for various values of the parameters α, β, and γ.

α	β	γ	$\lvert P \rvert / NGb^2$
0.002	1000	0.001	2158.1
0.003	1000	0.001	320.1
0.004	1000	0.001	26.7
0.005	1000	0.001	1.0
0.01	100	0.001	2.9
0.01	300	0.001	0.005
0.01	1000	0.005	9.5
0.01	1000	0.007	81.2
0.01	1000	0.010	2480.8

Table 1. Dimensionless pull-off force ($|P|/NGb^2$) for various values of the parameters α, β, and γ.

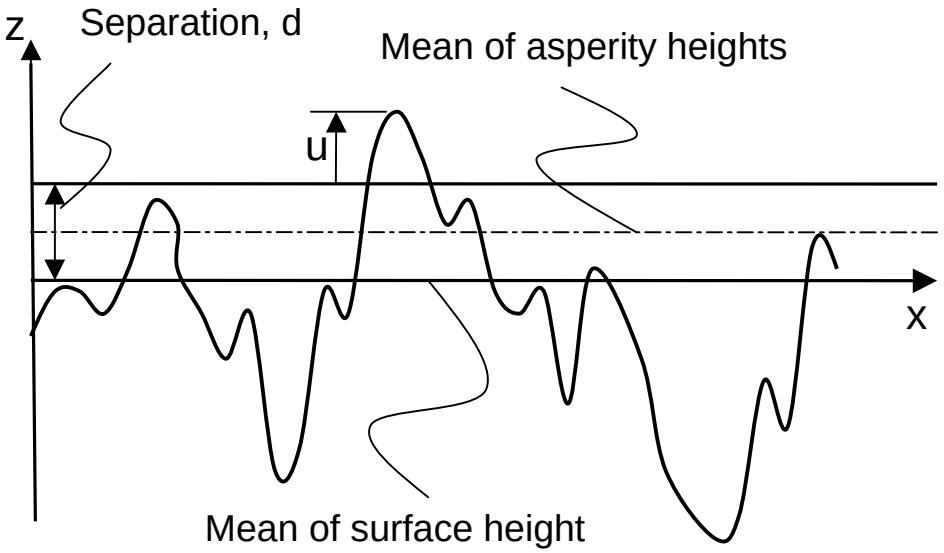

Figure 1. The topography of a rough surface and a smooth flat surface.

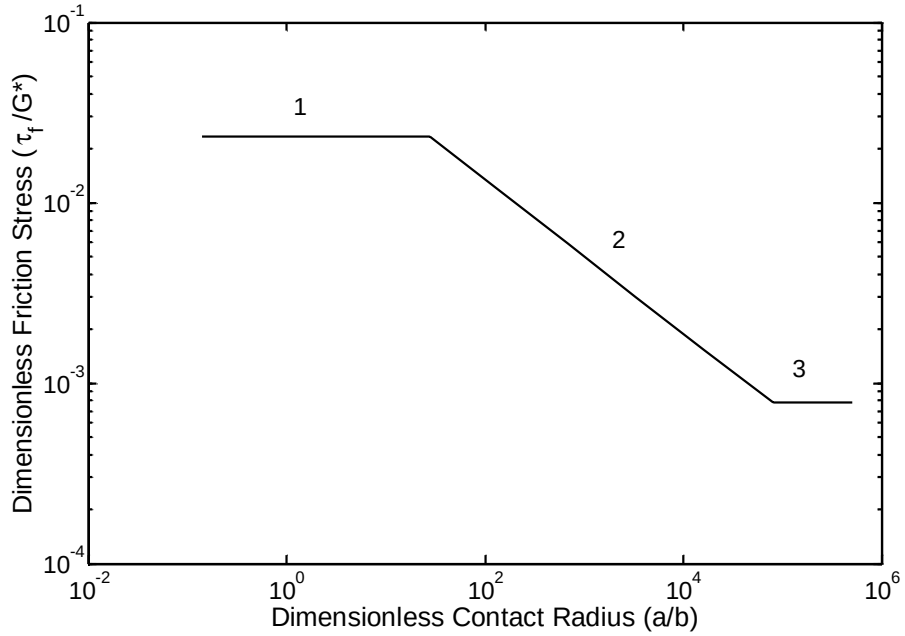

Figure 2. Relationship between the dimensionless friction stress and the dimensionless contact radius according to the HK model.

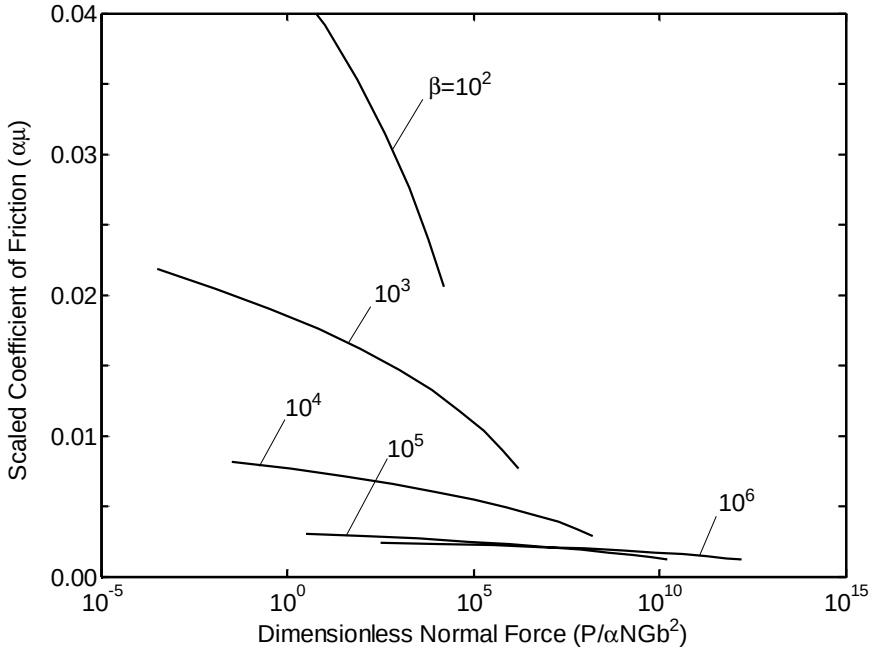

Figure 3. Scaled coefficient of friction ($\alpha\mu$) vs. scaled normal force ($P/\alpha NGb^2$) for various values of β, without adhesion (γ= 0).

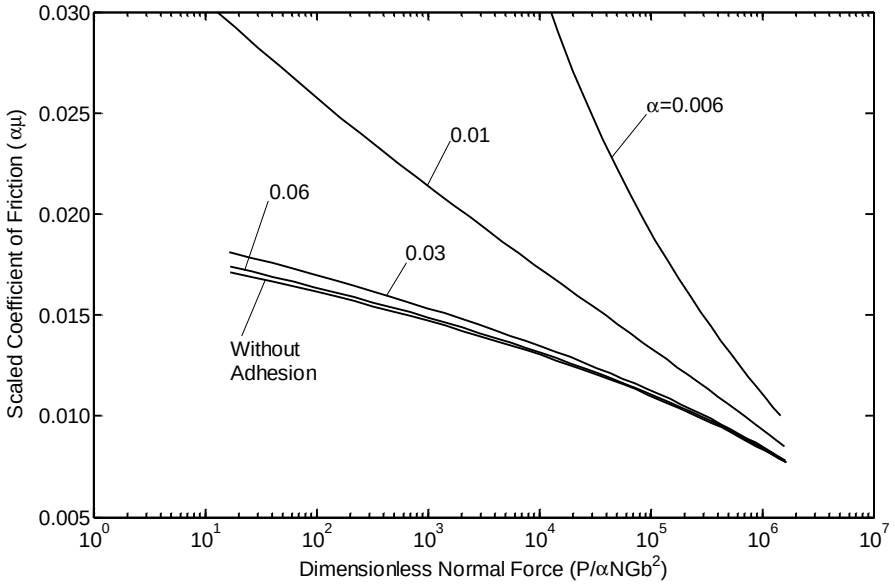

Figure 4. Scaled coefficient of friction ($\alpha\mu$) vs. scaled normal force ($P/\alpha NGb^2$) for various values of α, with γ=10^{-3}.

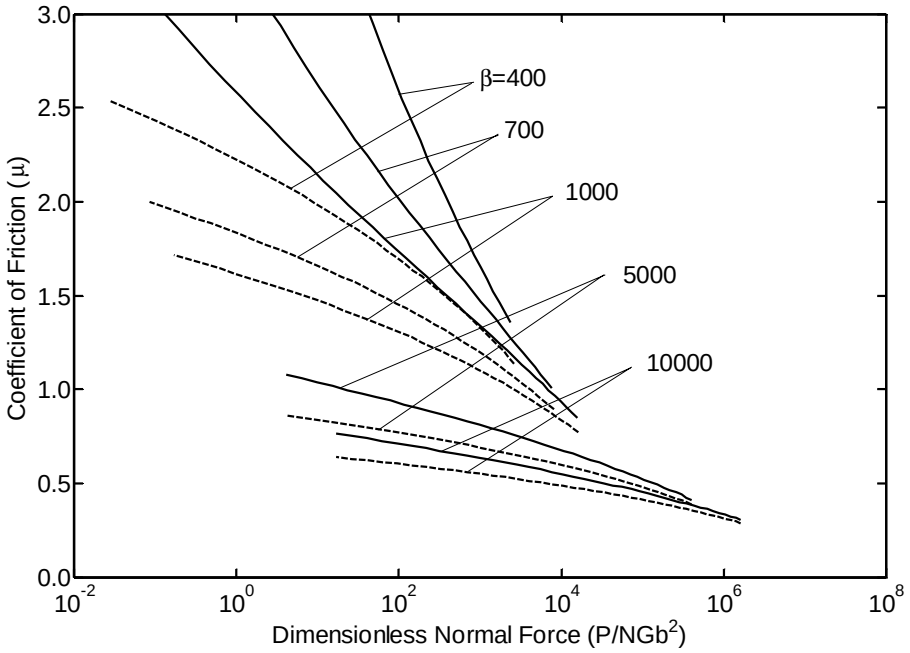

Figure 5. Coefficient of friction (μ) vs. the dimensionless normal force (P/NGb^2) for various values of the friction regime parameter β, with $\alpha = 0.01$, with adhesion ($\gamma = 10^{-3}$, solid lines) and without adhesion ($\gamma = 0$, dashed lines).

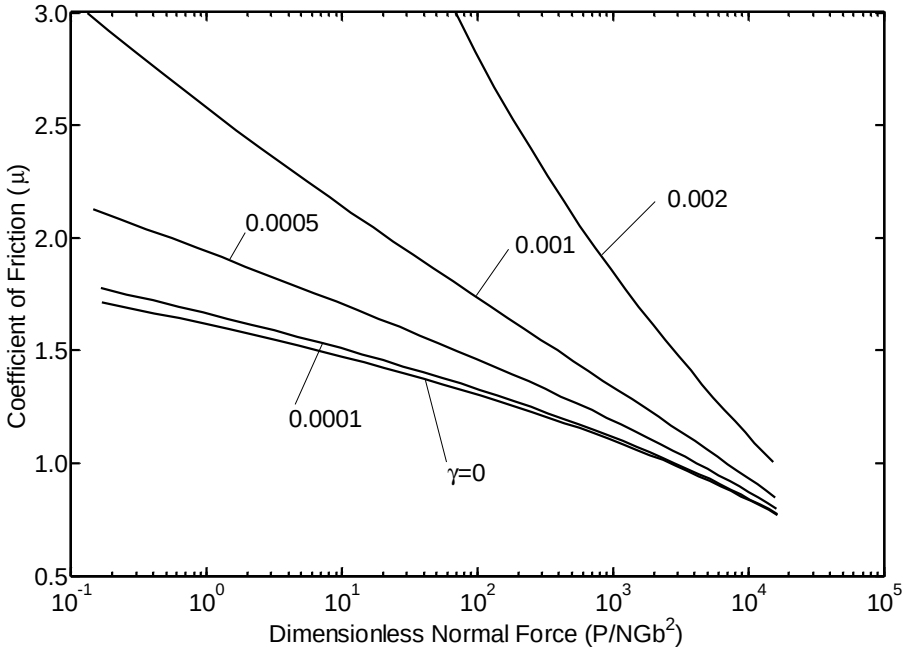

Figure 6. Coefficient of friction (μ) vs. the dimensionless normal force (P/NGb^2) for various values of the surface energy/compliance parameter (γ), with $\alpha = 0.01$ and $\beta = 1000$.

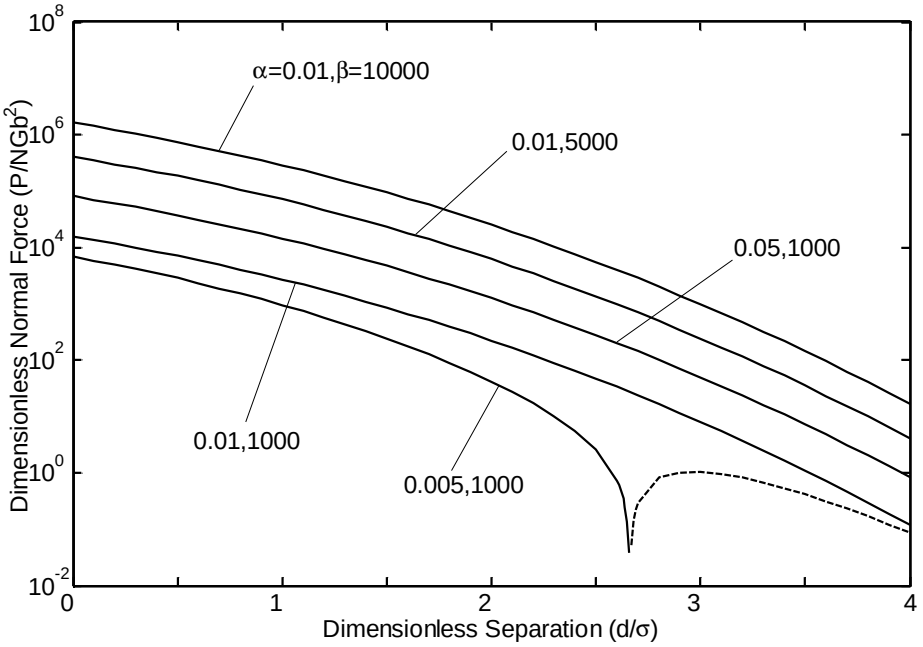

Figure 7. Dimensionless normal force (P/NGb^2) vs. dimensionless separation (σ/d), for various values of α and β, and with $\gamma = 10^{-3}$. Dashed lines indicate that the normal force is tensile.

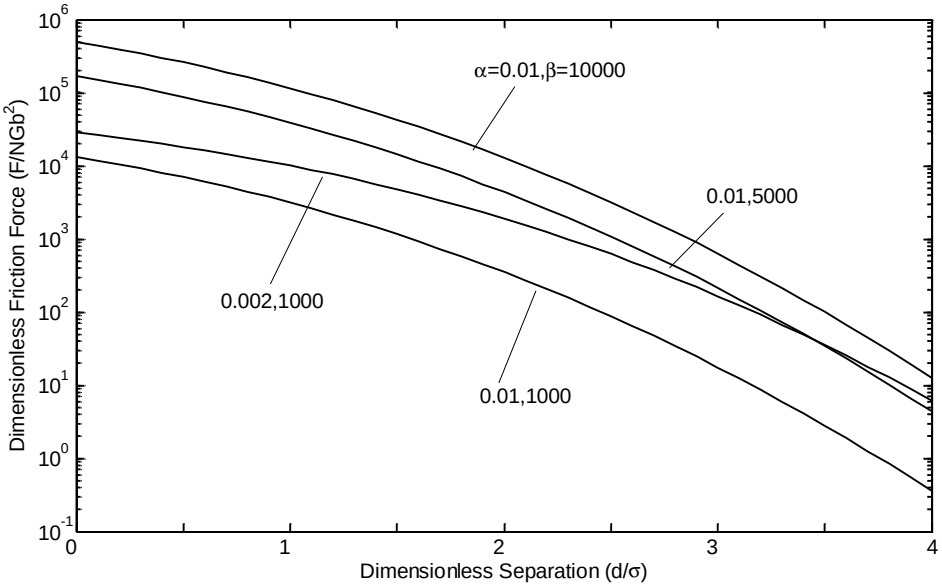

Figure 8. Dimensionless friction force (F/NGb^2) vs. dimensionless separation (σ/d), for various values of α and β, and with $\gamma = 10^{-3}$.

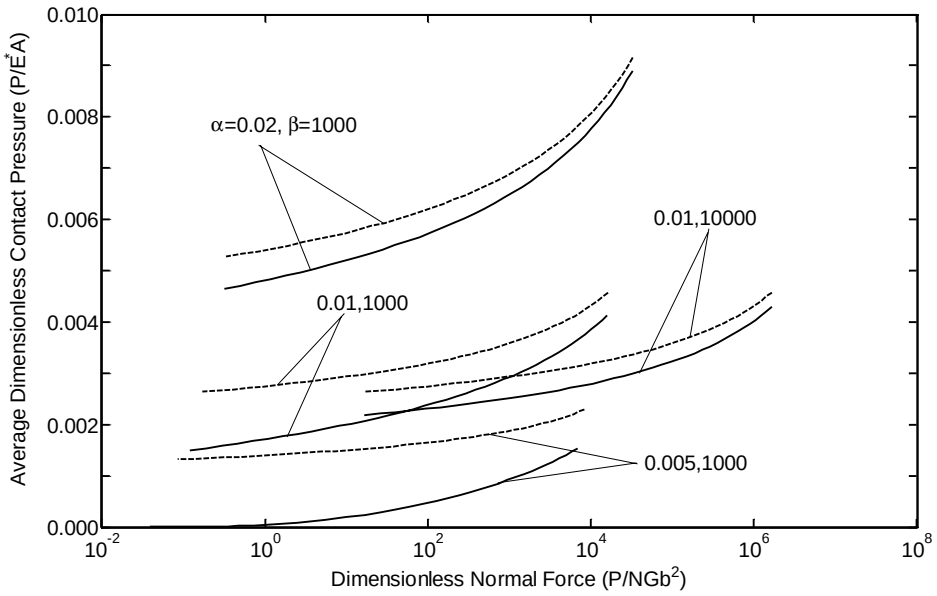

Figure 9. Dimensionless average contact pressure (P/E^*A) vs. dimensionless normal force (P/NGb^2), for various values of α and β, with $\gamma = 10^{-3}$ (solid lines), and $\gamma = 0$ (dashed lines).